A Simplified Method to Determine the 3D Orientation of an Injection Molded Fiber-Filled Polymer

G. Regnier, D. Dray, Eric Jourdain, Sabine Le Roux, Fabrice Schmidt

A Simplified Method to Determine the 3D Orientation of an Injection Molded Fiber-Filled Polymer

G. Régnier,[1] D. Dray,[1] E. Jourdain,[2] S. Le Roux,[2] F.M. Schmidt[2]
[1] *Arts et Métiers ParisTech 151 bd de l'Hôpital 75013, Paris, France*

[2] *Ecole des Mines d'Albi Carmaux, Route de Teillet 81013, Albi CT Cedex 09, France*

In short-fiber reinforced composites, it is widely accepted that the fiber orientation plays an important role on their overall physical and thermomechanical properties. To predict the properties of such composite materials, a full 3D fiber orientation characterization is required. A variety of destructive and nondestructive techniques have been developed, but all the methods have the same common point that they are very tedious and time consuming. Knowing that the fiber orientation induced by the flow remains mainly in the flow plane, an easier method has been performed for injection molded fiber-filled polymers. It is based on the simple 2D SEM image analysis of a specific 45°-oblique section plane. Then, the indetermination of fiber orientation from an ellipse mark analysis does not exist anymore. This novelty also turns out to be much more accurate. To achieve measurements over large composite samples, the method has been fully automated.

INTRODUCTION

In short-fiber reinforced composites, it is widely accepted that the microtexture plays an important role on their overall physical and thermomechanical properties. Among the primary microtextural parameters (such as fiber volume fraction, aspect ratio, or distribution), the fiber orientation is one of the most significant variables, as it governs the anisotropy of the composite. It strongly influences the macroscopic material behavior, especially its stiffness, thermal expansion, thermal conductivity, and viscosity [1–3].

The processing route highly controls the fiber orientation distribution. In the particular case of injection-molded polymers, two stages are successively followed: polymer filling into the mold cavity and polymer cooling under pressure, which generates a post-filling and aims at reducing the part shrinkage. A typical shell-core structure of the fiber distribution is induced by the flow results, where the fibers tend to align with the injection direction at skin and lie perpendicular to it at core [4, 5]. For such orientation-dependent material properties, the use of micromechanic models [6] enables to link the predicted local fiber distribution [7] to the local material behavior. In particular, to predict the properties of such composite materials, many theories begin by studying the properties of the unidirectional composite, then resort to an orientation averaging procedure [1, 8, 9] that requires a full 3D fiber orientation characterization. Therefore, methods for measuring the 3D distribution of filler inside the matrix are clearly of great importance.

Several techniques are based on radiation absorption. They include scanning contact microradiography [10], transmission light microscopy [11], microwave absorption [12], and the promising X-ray microtomography imaging, which is still very expensive and time consuming [13].

Other more original techniques are based on acoustic microscopy [14], light diffraction [15], or X-ray diffraction. The latter technique could be applied to the particular case of semicrystalline fibers such as polyaramid fibers, where the 3D fiber orientation can be determined from pole figures [16].

Nevertheless, the majority of the works, which are done on the fiber orientation determination induced by polymer processing, is based on reflection microscopy analysis. Among the different techniques, the most simple is the optical reflection microscopy [17–19], but it only provides the 2D orientation information in its most simple analysis, which is generally not sufficient. The use of confocal laser scanning microscopy [20, 21] gives cleverly the access to 3D fiber orientation distribution (FOD), although this technique seems difficult to perform. Some improvements on reflection microscopy analysis may enable 3D FOD. We have worked in this direction, and the experimental procedures are presented in the following section. A specific scanning electron microscopy (SEM) image analysis, firstly described by Avérous et al. [22], has been developed. The results of 3D fiber orientation

Correspondence to ; e-mail: gilles.regnier@paris.ensam.fr
Contract grant sponsors: Legrand; Moldflow; Solvay.

states are shown in the form of probability distribution functions or of components of orientation tensors in the section on SEM Shadow Method Analysis. Finally, still based on SEM analysis, this article presents a simplified technique for experimental determination of 3D orientation state, in the particular case of injection molded fiber-filled polymers (the Simplified 3D Method for Injection Molded Parts section): the principle consists of 2D image analysis on preferential sectioning to get much more faster and accurate measurements.

FIBER ORIENTATION DETERMINATION USING REFLECTION MICROSCOPY ANALYSIS

Fiber Orientation Modeling

The orientation of an individual fiber can be defined by 2 angles θ and ϕ or by Cartesian components of a vector $\vec{p}$ aligned parallel to the fiber in a system of axes where the axis Z is normal to a section plane (see Fig. 1):

$$\vec{p} = (\sin\theta\cos\phi,\ \sin\theta\sin\phi,\ \cos\theta). \tag{1}$$

For millions of fibers, it is impractical to specify the orientation of each fiber and an alternative is to use the probability distribution function $\psi(\theta,\phi)$ [1], which describes the probability of finding fibers with orientation (θ,ϕ) in the specimen [23]. The probability that a fiber will be oriented between the angles θ_1 and $\theta_1 + d\theta$ and ϕ_1 and $\phi_1 + d\phi$ is defined by:

$$P(\theta_1 \le \theta \le \theta_1 + d\theta, \phi_1 \le \phi \le \phi_1 + d\phi) = \psi(\theta_1, \phi_1)\sin\theta_1 d\theta d\phi. \tag{2}$$

Because two fibers at angles (θ,ϕ) and $(\theta - \pi,\phi + \pi)$ cannot be distinguished, the function has the following symmetry: $\psi(\vec{p}) = \psi(-\vec{p})$. The probability distribution function is a density function and, therefore, subject to a normalization condition:

$$\int_0^{\pi}\int_0^{2\pi} \psi(\theta,\phi)\sin\theta\ d\theta\ d\phi = 1. \tag{3}$$

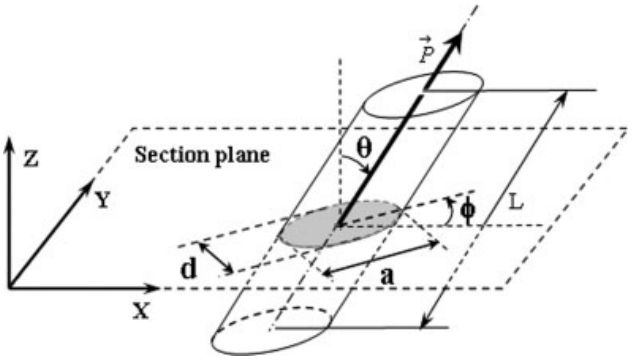

FIG. 1. Definition of fiber orientation.

However, the variation of probability as a function of either one of the two angles, what leads to the calculation of probability functions $P_\theta(\theta)$ and $P_\phi(\phi)$, can also give interesting information concerning the distribution of fibers. The experimental identification of these functions often leads to discrete distribution functions.

Although probability density functions provide a complete characterization of fiber orientation, they hold a considerable amount of information, and any calculation based on these data are highly computationally intensive. That is why the tensor description, which is a compact, general, and short formulation, is more widely used for fiber orientation characterization, especially in micromechanics models when the fiber orientation is taken into account. The second- and fourth-order orientation tensors $[a_2]$ and $[a_4]$, respectively, are generally needed [24], and they are calculated by forming dyadic products of the vector $\vec{p}$. The components of the second- and fourth-order orientation tensors are:

$$a_{ij} = \int_\Omega p_i p_j \psi(\vec{p}) d\vec{p} \quad \text{and} \quad a_{ijkl} = \int_\Omega p_i p_j p_k p_l \psi(\vec{p}) d\vec{p} \tag{4}$$

For a finite fiber number n, the global orientation tensors of a sample are obtained by averaging all individual fiber orientation:

$$a_{ij} = \frac{1}{n}\sum_{k=1}^{n} a_{ij}^k = \frac{1}{n}\sum_{k=1}^{n} p_i^k p_j^k \quad \text{and} \quad a_{ijkl} = \frac{1}{n}\sum_{k=1}^{n} p_i^k p_j^k p_k^k p_l^k. \tag{5}$$

For an individual fiber k, the coefficients of the second order orientation tensor $[a_{ij}^k]$ are equal to the well-known values:

$$\left[a_{ij}^k\right] = \begin{bmatrix} \sin^2\theta_k\cos^2\phi_k & \sin^2\theta_k\cos\phi_k\sin\phi_k & \sin\theta_k\cos\theta_k\cos\phi_k \\ \sin^2\theta_k\cos\phi_k\sin\phi_k & \sin^2\theta_k\sin^2\phi_k & \sin\theta_k\cos\theta_k\sin\phi_k \\ \sin\theta_k\cos\theta_k\cos\phi_k & \sin\theta_k\cos\theta_k\sin\phi_k & \cos^2\theta_k \end{bmatrix} \tag{6}$$

It is worth noting that the order of the orientation tensor is a way of changing the detail of the distribution description. It is clear that the use of second-rank orientation tensor is a reducing approach, as only five independent components characterize the orientation. Besides a second-rank orientation tensor does not lead to a unique distribution of fibers (whereas a given distribution leads to a unique orientation tensor). On the other hand, they represent a useful tool when modeling, because they are easily integrated in equations of mechanics.

It must be pointed out that for any fiber, the probability of intersection with a section plane normal to axis Z decreases when the misalignment angle θ increases and the fiber length reduces (see Fig. 1), leading to progressive undercounting of fibers when the angle θ increases.

To correct this bias, a weighting function must be applied to the measured data of each fiber k, and various forms of this function have been proposed by different authors [25–27]. In all cases, the function depends on the fiber length L and diameter d or on its aspect ratio L/d. In the simplest way [21], the probability F that a fiber k of finite length L and diameter d will intersect a section plane at the angle θ_k is determined by a simple geometry analysis (see Fig. 1):

$$F(\theta_k) = \frac{1}{L\cos\theta_k + d\sin|\theta_k|}. \tag{7}$$

The correction must be considered whatever the chosen type of orientation characterization. In particular, for discrete distribution functions, the probability P_θ of finding a fiber around angle θ (for $-\pi/2 \leq \theta \leq \pi/2$ and m intervals) is estimated by counting all the fibers around the angle θ ($\theta-\pi/m \leq \theta < \theta+\pi/m$), and by dividing it by the total number of fibers in the specimen. It can be shown [21] that $P_{\theta\text{corrected}}$, an unbiased estimate of the probability P_θ, has to be weighted as:

$$p_{\theta\text{corrected}}(\theta) = \frac{P_\theta(\theta)F(\theta)}{\sum_{i=1}^{m} P_\theta(\theta_i)F(\theta_i)}. \tag{8}$$

The components a_{ij} of the unbiased estimate of the second-rank orientation tensor must be weighted as:

$$a_{ij} = \frac{\sum_{k=1}^{m} F(\theta_k)a_{ij}^k}{\sum_{k=1}^{m} F(\theta_k)}. \tag{9}$$

The unbiased fourth-rank orientation tensor can be determined in the same way.

Fiber Orientation Determination from Reflection Microscopy Analysis

If a cross-section normal to axis Z is considered, the intersection of a fiber with a section plane is an ellipse (see Fig. 1). The use of an image analysis software enables to identify each fiber as an ellipse and automatically determines the ellipse center coordinates (x_c,y_c), its major and minor axes a and b respectively, as well as its in-plane orientation angle ϕ. However, an ambiguity remains as for the orientation of the fiber, which can have two equally possible positions: a fiber oriented at $+\theta$ and $-\theta$ (equivalent to $-\theta + \pi$) yields the same cutting ellipse; so, the sign of angle θ stays undetermined. Consequently, some components of the second-rank orientation tensor (namely the off-diagonal components a_{13} and a_{23}, see *Eq. 6*) remain undetermined. As a consequence, the whole orientation state cannot be fully described by the information from one cross-section, unless a priori knowledge of a specific fiber orientation distribution is supposed. To remove this ambiguity on the sign of θ, a variety of destructive and nondestructive techniques have been developed for measuring FOD. Some authors then suggest deriving 3D FOD by combining data from two orthogonal plane sections [25] or from two inclined cross-sections [28]; others claim that three orthogonal sections are required [20]; eventually others propose to perform two consecutive closely spaced cross-sections of a specimen [29]. The experimental implementation of these last approaches is practically time-consuming and difficult, as the specimen must be removed between two section analyses.

Another variety of methods consists in guessing the orientation of the fiber under the matrix. A specific optical technique was proposed to obtain three-dimensional FOD [30], whereby a transparent matrix with opaque fibers is observed with an optical microscope. The requirements for the material colors and the depth restriction highly limit the use of this method. Confocal laser micrography is without any doubt an efficient method [20, 21], but the method requires a very specific equipment. Then, a 3D fiber orientation by shadow SEM analysis was first introduced by Avérous et al. [31] and reworked by Saint-Martin et al. [32] and Wesselmann [33]. This latter methodology, which has appeared to us less tedious, has been developed and is presented in the next section.

Principle of 3D Fiber Orientation Determination by Shadow SEM Analysis

As a first remark, both phases often appear of the same color with optical microscopy, while the images obtained by SEM always show a higher fiber/matrix contrast with a well-defined interface. Very well polished samples should be observed via a source of retrodiffused electrons, in which nearly a binary image is obtained, where the fibers appear in white on a dark background. If a high voltage tension is applied (typically 20 kV), a grey shadow appears at one of the extremities of the ellipse (see Fig. 2), due to the low amount of matrix covering the fiber. Then the method consists of observing the same SEM image with two different thresholds by the mean of

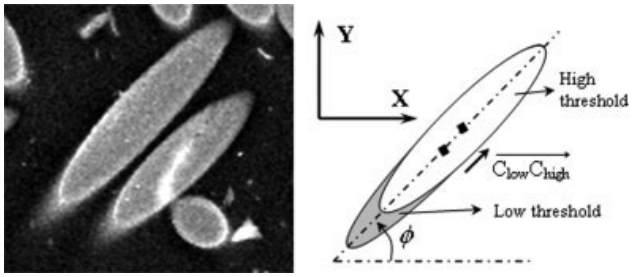

FIG. 2. Determination of the sign of angle θ thanks to the fiber shadow.

the image analysis system: a low threshold that includes the shadow in the fiber image, and a high one that excludes it (see Fig. 2). Some mathematical morphology operators, such as erosion-reconstruction, are then used to remove the small incomplete fiber ellipses on the binary image.

By fitting ellipses to the fiber cross-sections observed within these thresholds, we can obtain the respective ellipse characteristics. The displacement vector of the ellipse centers $\overrightarrow{C_{low}C_{high}}$ is evaluated for each matched fiber and with a rule determining in which condition the angle θ is positive or negative.

Experimental

Composite plaques (60×60 mm^2 squares) of two different thicknesses e (namely $e = 1$ and 3 mm) were injection molded on the DK Codim 175-400 injection press, through a fan-gate of 0.8 mm for 1 mm-thick plates and 2 mm for 3 mm-thick plates. The material pellets were supplied by Solvay® and two grades of glass fiber filled polyarylamide are considered: IXEF™ 1002 that contains 30 wt% of glass fiber and IXEF™ 1022 that contains 50 wt% of glass fiber. The diameter of fibers is 10 μm and the mean fiber length after injection is about 0.25 mm. The samples for fiber orientation analysis were taken in the center of the plate at 20 mm from the gate.

The reliability of fiber orientation data highly depends upon the quality of the surface preparation of the sample. Pressure, time, and disk rotation speed during each polishing stage, as well as the grade of the first polishing disk are important parameters to reduce cracking of the fibers and to enhance the contrast in preparation for image analysis. For polyarylamide composites, the best polishing protocol is described in Table 1.

To measure the fiber orientation, a section plane is cut (at different possible angles) through the plaque and consequently two systems of axes must be distinguished: the global injection coordinate system, namely (1,2,3), where direction 1 represents the flow direction, direction 2 the transverse direction and direction 3 the thickness direction, and the section plane system of axes, namely (X,Y,Z) where Z is normal to the section plane and X in the plane (1,2) of the injection molded plate (see Fig. 3). The result

TABLE 1. Polishing protocol for polyarylamide composites.

Polishing disk grade	Speed (m/s)	Pressure (N/mm^2)	Time (min)	Specific conditions
800	2.6	0.42	2	Water
1200	2.6	0.42	2	Water
2400	2.6	0.08	4	Water
4000	2.6	0.08	4	Water
OPS	1.6	0.01	5	–

OPS: colloidal silica suspension (0.04 μm particles).

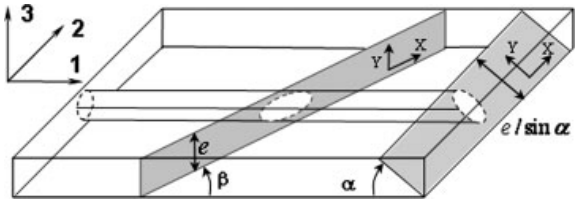

FIG. 3. Two sectioning planes whose normals are (sin β, $-\cos\ \beta$, $0)_{1,2,3}$ for the plane on the left of the figure and (sin α, 0, cos $\alpha)_{1,2,3}$ for the plane on the right of the figure.

is that the orientation data $(\theta,\phi)_{X,Y,Z}$ of a fiber measured with respect to a section plane will have to be transformed to the frame of reference, so that this same fiber is characterized by angles $(\theta',\phi')_{1,2,3}$ in the injection system of axes. The values of θ span the $[0,\pi]$ range and ϕ span the $[-\pi/2,\pi/2]$ range, so that the whole space is covered.

For hundreds of fibers though, it is impractical to manually specify the orientation of each fiber and to identify the matching ellipse pairs. To facilitate these tasks, an alternative is to automate the process of localization and fiber center following. For this reason, an in-house program was then developed with the use of Matlab® software coupled to the image analysis system Micro Vision System® to automate the procedure of collecting data on many fibers efficiently. The software was validated with well-chosen computer-generated images.

For injection molded plates, the thickness of the section plane was divided into several successive layers. The orientation results on each layer are determined by six images analyzed separately. Each image has a dimension of 0.27×0.20 mm^2, is defined by 400×300 pixels, and contains about 70 fibers. To have a more precise fiber counting, the images can be stitched [19]. We proceed as follows: an overlap of 0.05 mm (75 pixels) between the images is set. At present, the partially seen fibers on the image edges are removed manually to avoid errors, but the overlap of the adjoining image should allow taking into account most of the fibers eliminated manually (only fiber centered on the overlap zone with a θ angle larger than 78° cannot be counted). All fiber characteristics are stored (coordinates in the sectioning plane and orientation), so that it is easy to eliminate the fibers counted twice.

For the SEM shadow technique, there is a difficulty to identify the ellipses belonging to the same fibers within the two binary images. This identification is performed by using the two fiber datasets and looking for the minimum differences between ellipse center coordinates (x_c,y_c). Practically, two ellipses correspond to the same fiber if Δx_c and Δy_c are smaller than $0.2d$, where d is the diameter of the fiber.

SEM SHADOW METHOD ANALYSIS

In this section of the article, sectioning is performed perpendicular to the injection direction. It is worth noting

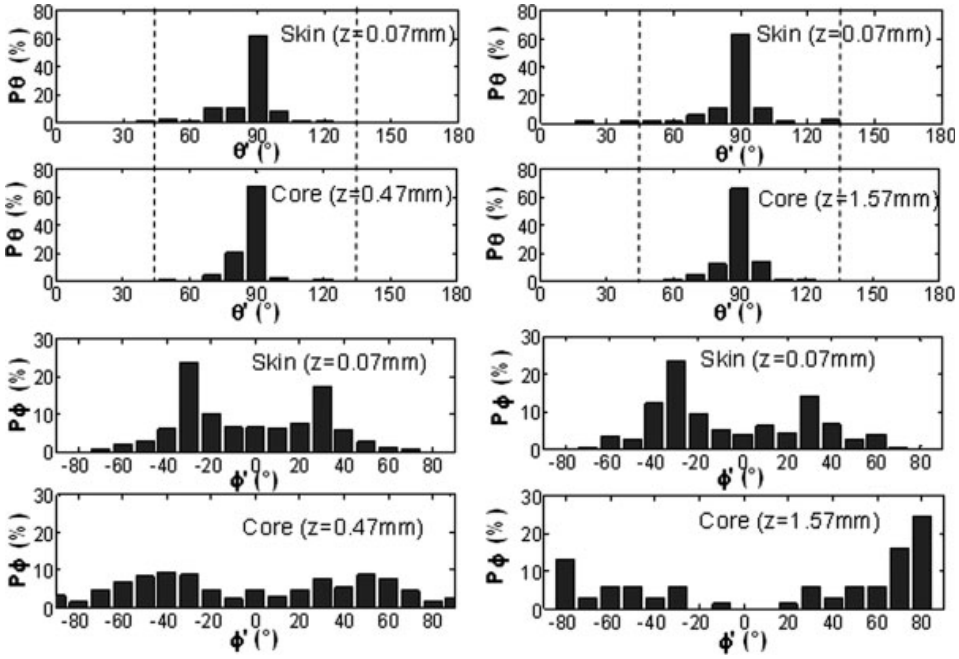

FIG. 4. SEM shadow technique: corrected fiber length FOD as a function of either one of the two angles ϕ' and θ' of 30% fiber-filled polyarylamide plates; cutting section plane normal to flow direction. Left graphs: FOD for 1 mm-thick plates; right graphs: FOD for 3 mm-thick plates.

the importance of the correction factor F (*Eq. 7*) on angle θ: when sectioning is performed perpendicular to the flow direction and due to the core-shell structure of the distribution, there is an undercounting of fibers at the core (as the fibers lie in the section plane) and an overcounting at skin (as they are perpendicular to the section plane).

The measured FOD for 1- and 3-mm-thick plates of 30 wt%-fiber reinforced polyarylamide are described in Fig. 4. The thickness was divided into seven successive layers for 1-mm thick plates, 21 layers for 3-mm thick plate, but only the fiber distribution at skin ($z = 0.07$ mm from the plate's surface) and at core ($z = 0.47$ mm for 1 mm-thick plate and 1.57 mm for 3 mm-thick plate) is shown in Fig. 4. As expected, it clearly appears that θ' values are mostly equal to $\pi/2$, which means that the fibers lie mainly in the injection plane. Besides, the calculation of the global second-rank orientation tensor of the sample confirms this fact, as the a_{33} component has a very low value (close to 0) for both polyarylamide grades (Table 2).

At core, ϕ' tends to ± 90 for 3 mm-thick plates, then fibers tend to be normal to flow direction. This core-shell structure, which is very pronounced for 3 mm-plates, does not exist for 1 mm-plates. However, conclusions as for angle ϕ' are not so obvious: the variation of ϕ' values in the skin through thickness (see Fig. 4) would imply that during injection, the fibers are not oriented in the flow direction, but are somehow deviated at $\pm 30^\circ$ from direction 1. This fiber orientation distribution was not confirmed by observing polished crossed section parallel to the injection plaques in the skin region: only a maximum for $P\phi$ appears in the flow direction. One may rather suppose that a systematic measurement error of our image analysis system is implied when sectioning is performed perpendicularly to the flow direction.

Two main linked reasons can explain this systematic error, but in any case the principle of the shadow method is not in question. As most of the fibers are oriented in the flow direction after injection, they consequently appear as circles or quasicircles in a section plane perpendicular to flow direction. Firstly, let us consider a single fiber cut in this classical section plane normal to flow direction. The fiber direction in the injection axis reference (1,2,3) is given by the two angles ϕ' and θ', which can be determined by the measurement of ellipse dimensions d, a, and ϕ in the normal section plane (see Fig. 1):

$$\tan\phi' = \pm\cos\phi\sqrt{\left(\frac{a}{d}\right)^2 - 1}$$
$$\cos\phi' = \sin\phi\sqrt{1 - \left(\frac{d}{a}\right)^2}. \tag{10}$$

A small variation of the dimension ratio d/a induces a large variation of ϕ' and θ' angle. The derivatives of ϕ' and θ' with respect to d/a are even infinite for $d/a = 1$. In Fig. 5, the possible deviation of ϕ' is determined for fibers, which lie in the injection plane, according to *Eq. 13* and our measurement errors for ellipse dimensions ($\pm$ 0.6 μm). For a given value of angle ϕ', the lower and upper error limits are defined for a minimum and a maximum possible ratio d/a due to the measurement error. A large deviation can be made for low values of ϕ', that is

TABLE 2. Corrected length fiber tensors for fiber-filled polyarylamide injection molded plates simplified method determination.

Fiber content (wt%)	Thickness (mm)	Normal direction of section plane	Orientation tensor in system axis (1,2,3)
30	1	$(1,0,0)_{1,2,3}$	$\begin{bmatrix} 0.59 & -0.04 & -0.002 \\ -0.04 & 0.37 & 0.005 \\ -0.002 & 0.005 & 0.04 \end{bmatrix}$
30	3	$(1,0,0)_{1,2,3}$	$\begin{bmatrix} 0.55 & -0.02 & 0.003 \\ -0.02 & 0.41 & -0.006 \\ 0.003 & -0.006 & 0.04 \end{bmatrix}$
30	1	$(1,0,1)_{1,2,3}$	$\begin{bmatrix} 0.79 & 0.01 & 0.05 \\ 0.01 & 0.18 & 0.006 \\ 0.05 & 0.006 & 0.03 \end{bmatrix}$
30	3	$(1,0,1)_{1,2,3}$	$\begin{bmatrix} 0.64 & 0.006 & 0.04 \\ 0.006 & 0.33 & 0.003 \\ 0.04 & 0.003 & 0.03 \end{bmatrix}$
50	1	$(1,0,1)_{1,2,3}$	$\begin{bmatrix} 0.76 & 0.07 & 0.001 \\ 0.07 & 0.22 & -0.0008 \\ 0.001 & -0.0008 & 0.02 \end{bmatrix}$
50	3	$(1,0,1)_{1,2,3}$	$\begin{bmatrix} 0.65 & -0.04 & 0.02 \\ -0.04 & 0.32 & -0.01 \\ 0.02 & -0.01 & 0.03 \end{bmatrix}$

for values of d/a close to 1. A maximum error occurs at about 30°: it corresponds to the maximum value of the lower limit for which the measured ratio d/a can be equal to 1. Secondly, the limited and discrete resolution of the digital camera contributes also to this systematic error. The magnification of the image is such that 16 pixels correspond to the fiber diameter. If we suppose that major and minor axes differ by only one pixel, it is then very unlikely that the calculated value of angle ϕ' will be less than $arcos(15/17) = 28°$.

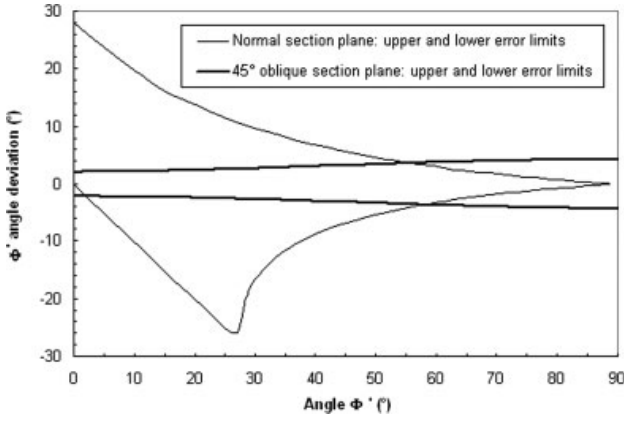

FIG. 5. Upper and lower error limits of ϕ' angle for a fiber laying in the injection plane (1,2) for two sectioning planes: normal to injection flow (direction 1) and 45° oblique section (right plane of Fig. 3).

Error on orientation data is thus easily performed when we have to analyze circles. It is possible to reduce the error by increasing the resolution of the camera (800 × 600 pixels or more is available now) or the magnification. But for high magnification, an automatic scheme is really needed to stitch the images together and to take the partially seen fibers into account [19]. As fibers are mainly oriented in the flow direction in the part skin, the precision of the orientation determination can be improved when the angle α between the normal of the sectioning plane and the flow direction is different from 0° (see Fig. 3) [34]: the fibers, circular in cross-section, will appear as ellipses. Researchers have thus achieved better angular resolution on orientation angles θ' and ϕ' by preferential oblique sectioning to flow direction, typically in the range 30° to 80° [18].

SIMPLIFIED 3D METHOD FOR INJECTION MOLDED PARTS

Principle of the Method

Let us consider an angle of 45° between the flow direction and the normal of the sectioning plane. For easier handling, it was first suggested to perform sectioning normally to the (1-2) part plane (left area in Fig. 3) as Yurgartis [35], instead of an oblique plane section from the plaque plane (right area in Fig. 3), believing both sec-

tioning were equivalent. However, after careful consideration it turns out that because of thickness, sectioning is more advantageous.

For one fiber cut in the oblique sectioning plane, the fiber direction in the injection axis reference (1,2,3) is given by:

$$\tan\phi' = -\frac{\sqrt{2}\cos\phi\sqrt{1-\left(\frac{d}{a}\right)^2}}{\left(\frac{d}{a}\right)+\sin\phi\sqrt{1-\left(\frac{d}{a}\right)^2}}$$
$$\cos\theta' = \frac{1}{\sqrt{2}}\left(\left(\frac{d}{a}\right)-\sin\phi\sqrt{1-\left(\frac{d}{a}\right)^2}\right). \quad (11)$$

As the image analysis system seems to be more accurate in the determination of $\phi_{X,Y,Z}$ (a precision of $\pm 3^\circ$ for $d/a < 0.8$ has been determined experimentally), the possible deviation of angle ϕ' for fibers, which lie in the injection plane, are lower than $\pm 4^\circ$ (see Fig. 5), while the error on angle θ' remains lower than $\pm 7^\circ$. For one fiber, the maximum error on diagonal terms of the second order orientation tensor remains less than 0.06 and 0.1 for non-diagonal terms. If the same standard deviation of orientation tensor coefficient is supposed for all fibers, the standard deviation on the mean orientation tensor coefficients should be roughly the standard deviation determined for one fiber divided by the square root of the number of fibers. Then a very precise evaluation of the second orientation tensor can be done with only 100 fibers.

Secondly, when an oblique sectioning is done, the section plane has a wider thickness than the plate's thickness ($e/\cos\alpha$). As our images have a constant height of 0.2 mm, the number of layers in the whole thickness is larger. This point is of interest when studying the variation of the fiber orientation through thickness.

Another point that deserves to be highlighted is as follows. According to the orientation results on injection molded plates by shadow SEM analysis (SEM Shadow Method Analysis section), which are consistent with literature results [5], we know that most of the fibers lie in the injection plane. From the distribution of angle θ' in Fig. 4, we see that all the fibers can actually be contained between two planes oriented at $\pm 45^\circ$ from the injection plane, and what corresponds to θ' values comprises between 45° and 135°. This observation is actually very useful, because considering a 45°-oblique sectioning through thickness constitutes a simple criterion for the determination of the sign of θ in the section plane system of axes (X,Y,Z) (see Fig. 6). Indeed a fiber can have two possible orientations $(\theta,\phi)_{X,Y,Z}$ and $(-\theta,\phi)_{X,Y,Z}$. Once transformed to the frame of reference, the fiber will also have two possible values of θ'. However, as we have the condition that $\theta' \in [45^\circ, 135^\circ]$, only one value will satisfy it and the sign of θ is easily determined without the need of following the fiber into the bulk material. This implies that for the fiber orientation measurement, only one image is required, i.e., no low and high thresholds need to be applied to the SEM micrograph.

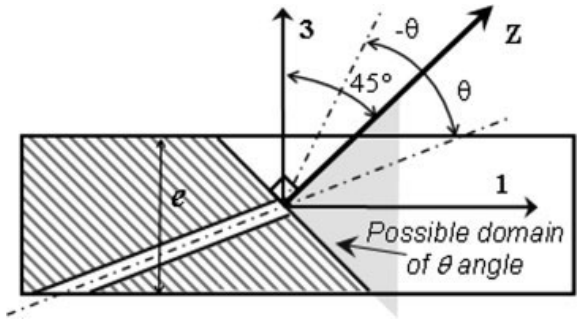

FIG. 6. Possible domain of θ angle in the case of injection-molded plates.

However, the simplified method has a drawback. The precision of the orientation measurement is not the same for fibers not lying in the injection plane. The fibers oriented on either side of the injection plane, at 30° and 120°, for example, will appear on the oblique section plane, respectively, as quasicircles and large deformed ellipses. Nevertheless, a very small amount of fibers is concerned for injection molded plates.

This simplified technique is applicable in the particular case of injection molded plates, because the fibers are oriented around the injection plane. For more complex-shaped regions of injection molded parts (such the base of a rib or a boss for example), the method would not be available anymore, but the shadow SEM technique can be applied with a sectioning plane in which most of the fibers are not seen as circles but as ellipses. It is worth noting that for injected plates, if sectioning was performed normally in the direction (1,1,0), it would not be possible to apply the technique neither because the fibers are oriented everywhere in the (1,2) injection plane.

Results

The FOD is studied through the plate's thickness, which is divided into several layers. Here again for convenience, only the results in the skin layer as well as in the core layer are shown. For 1 mm-thick plates of 30 wt% fiber-filled polyarylamide plates, the fibers lie in the injection plane ($\theta' = 80 - 90^\circ$) and are preferentially oriented in the flow direction all through the thickness (see Fig. 7), except in the core region where the distribution is quite large. For 3 mm-thick plates though, the fibers are still as a majority included in the injection plane. At skin, they are mostly oriented parallel to the injection direction, whereas very few fibers are oriented in the flow direction at core (see Fig. 7).

The $\pm 30^\circ$ orientation of the fibers that we observed when sectioning was performed perpendicularly to injection direction (see Fig. 4) has completely disappeared. It proves the systematic measurement error that was

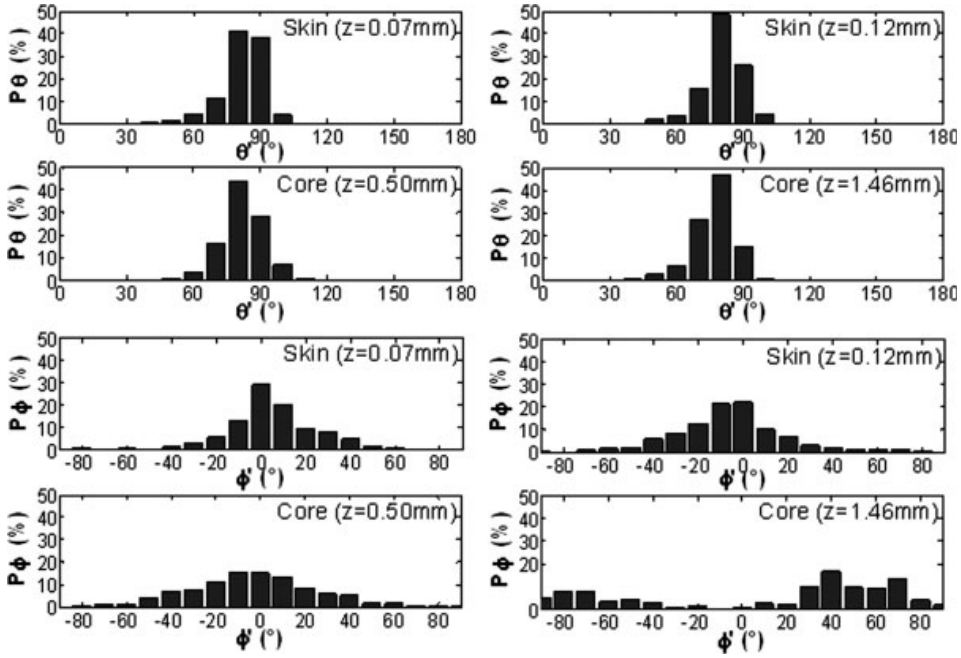

FIG. 7. Simplified method: corrected fiber length FOD as a function of either one of the two angles ϕ' and θ' of 30% fiber-filled polyarylamide plates. Cutting section plane normal to $(1,0,1)_{1,2,3}$ vector. Left graphs: FOD for 1 mm-thick plates; right graphs: FOD for 3 mm-thick plates.

assumed in the previous section and the reason is a default inherent in the image analysis system when circles have to be analyzed. Indeed when sectioning is carried out at 45°, as no circle (or very few) appears in the section plane, the effect of the bias is much more negligible.

Moreover, the corresponding orientation tensors lead to higher a_{11} component compared to sectioning at 90° (Table 2). These results are actually much more realistic, first because the thinner the injected parts, the more oriented in the flow direction the fibers are. Beside in-injection-plane sectioning was performed, and the components of the measured orientation tensors are in accordance with the ones obtained with a section plane at 45°. For comparison, Fig. 8 depicts the variation of a_{11} components through thickness for 30 wt% fiber-reinforced polyarylamide, when sectioning is performed in the injection plane, as well as at 45° and at 90°. We clearly see that sectioning normally to injection flow underestimates the a_{11} values, whereas sectioning at 45° yields results that are very close to the ones we obtain with in-injection-plane sectioning.

To have an idea of the influence of the fiber volume fraction on the fiber orientation, the FOD has been measured for a higher fiber content (50 wt% fiber-reinforced polyarylamide). The corresponding histograms for 1-mm and 3-mm thick injected plates are represented in Fig. 9

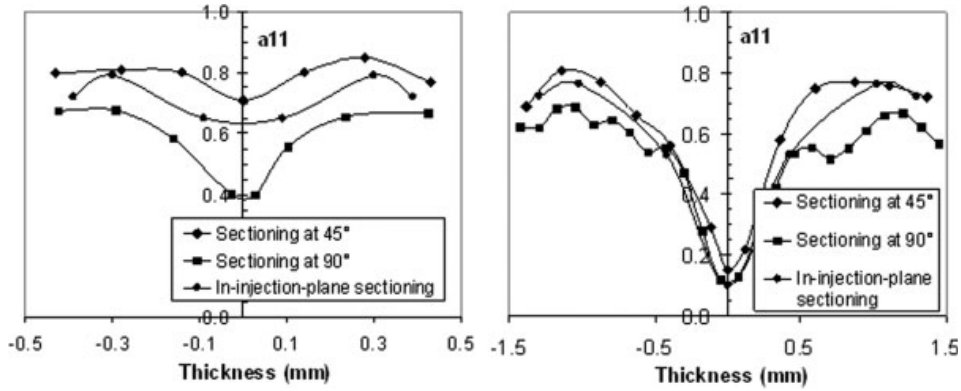

FIG. 8. Simplified method: through thickness variation of a_{11} measured by three different sectioning, for 30% fiber-filled polyarylamide plates. Left graph: a_{11} for 1 mm-thick plates; right graph: a_{11} for 3 mm-thick plates.

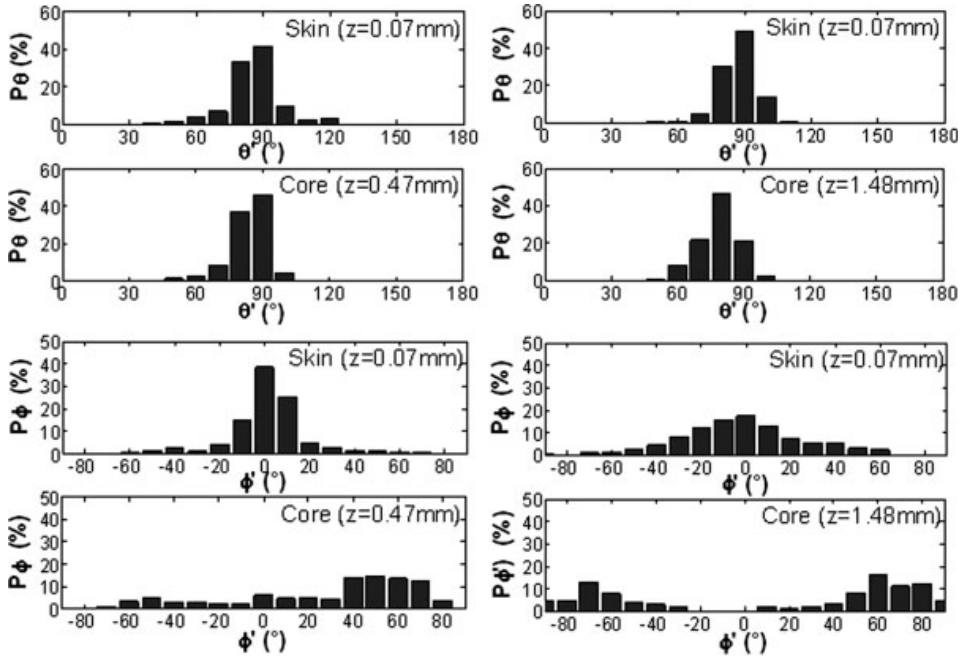

FIG. 9. Simplified method: corrected fiber length FOD as a function of either one of the two angles ϕ' and θ' for 50% fiber-filled polyarylamide plates; cutting section plane normal to $(1,0,1)_{1,2,3}$ vector. Left graphs: FOD for 1 mm-thick plates; right graphs: FOD for 3 mm-thick plates.

and the corresponding orientation tensors are shown in Table 2. The difference between the tensor data for the two materials is less than the measurement error, but significantly different fiber orientation distributions in the thickness can lead to the same average value. Nevertheless, this is an interesting result by itself, since it suggests that macroscopic fiber orientation behavior is not strongly dependent on fiber volume fraction.

After this, the 3D FOD has been experimentally measured for 1- and 3-mm thick plates of injection molded fiber-filled polymers. We can get quite simply the shape of the distribution all through the part's thickness. In particular, it clearly appears that the plaque's thickness plays a significant role in the distribution of the fibers into the matrix, while the fiber content has a much more negligible influence.

CONCLUSION

The shadow SEM analysis technique enables the efficient three-dimensional determination of fiber orientation from a single polished section with good accuracy: there is no longer any ambiguity as to the direction of one fiber and a complete orientation description can be measured. The procedure, applicable to any fiber-reinforced polymer composite, has been fully automated making it possible to collect results over large areas within relatively fast time scales. A particular attention has to be given to the inaccuracy of the orientation determination of fibers, whose axes are close to the sectioning plane normal. Therefore, the sectioning plane should not be normal to the main fiber orientation.

In the particular case of injection-molded fiber-filled polymer, a particular distribution of the fibers is induced by the flow and the result is that most of the fibers are contained around the injection plane (actually they lie between two planes oriented at $\pm 45^\circ$ from the injection plane). Consequently, when an oblique sectioning is performed at a preferential angle (namely 45°), a simple criterion can be applied to determine the sign of angle θ' from a single polished section and from a unique SEM image analysis (or from an optical microscopic image analysis the image contrast is sufficient): the measurements are faster than by the shadow SEM analysis technique (less manual processing), and above all these are easier and more precise. The methodology has been successfully applied to obtain 3D fiber orientation distribution within a set of short glass fiber polyarylamides, with no biased distribution data for near-zero values of angle ϕ': this technique appears to be very effective in reducing angle measurement uncertainty, especially for fibers oriented in the flow direction.

Local or global orientation tensors can be fully measured, either by the simplified 2D technique for injection-molded plane surfaces, or by the shadow technique for more complex 3D orientation distribution. The image acquisition on SEM is the same for the two techniques, only the image processing differs. Nevertheless, the use of the simplified method allows setting a lower voltage tension, which avoids fiber shadows and defines the fiber outlines better. These orientation characterization tools are useful

in many micromechanics models, when the fiber orientation has to be taken into account. However, a different representation of the fiber distribution can be obtained, as the FOD is a function of either one of the two angles θ' and ϕ', depending on the need of the operator.

Nevertheless, it is worth reminding that the reliability of fiber orientation data is strongly dependent upon the quality of surface preparation of the sample. Hence, the results are highly dependent upon the quality of images, the performance of the analysis system, as well as the accuracy of the 2D image analysis.

ACKNOWLEDGMENTS

The authors wish to thank H. Alglave, J. Correa, D. Delaunay, R. Fulchiron, S. Karpp-Pfordt, P. Kennedy, M. Laplanche, R. Le-Goff, V. Leo, J.M. Rossignol, and R. Zheng for the enriching discussions during the FISH (FIber filled polymers: injection and SHrinkage) project.

REFERENCES

1. S.G. Advani and C.L. Tucker III, *J. Rheol.*, **31**, 751 (1987).
2. M.L. Dunn and H. Ledbetter, *Mater. Sci. Eng.*, **A285**, 56 (2000).
3. J. Wang and P. Pyrz, *Comp. Sci. Technol.*, **64**, 925 (2004).
4. P. Singh and M.R. Kamal, *Polym. Compos.*, **10**, 344 (1989).
5. R. Bailey and B. Rzepka, *Intern. Polym., Process.*, **VI**, 35 (1991).
6. D. Dray, D.P. Gilormini, and G. Regnier, *Comp. Sci. Technol.*, **67**, 1601 (2007).
7. M. Vincent, T. Giroud, A. Clarke, and C. Eberhardt, *Polymer*, **46**, 6719 (2005).
8. B. Mlekusch, *Comp. Sci. Technol.*, **59**, 911 (1999).
9. A. Gusev, M. Heggli, H.R. Lusti, and P.J. Hine, *Adv. Eng. Mater.*, **4**, 931 (2002).
10. M.W. Darlington and P.L. McGinley, *J. Mater. Sci. Lett.*, **10**, 906 (1975).
11. M.J. Folkes and H.A. Potts, *J. Mater. Sci. Lett.*, **4**, 105 (1985).
12. K. Urabe and S. Yomoda, *Adv. Comp. Mater.*, **1**, 193 (1991).
13. F. Desplentere, S.V. Lomov, D.L. Woerdeman, I. Verpoest, I.M. Wevers, and A. Bogdanovich, *Comp. Sci. Technol.*, **13**, 1920 (2005).
14. F. Lisy, A. Hilter, E. Baer, E.J.L. Katz, and A. Meunier, *J. Appl. Polym. Sci.*, **52**, 329 (1994).
15. F. Polato, P. Parrini, and G. Gianotti, *Adv. Comp. Mater.*, **2**, 1050 (1980).
16. S. Lim, T. Kikutani, J.L. White, and T. Kyu, *Adv. Polym. Technol.*, **8**, 325 (1998).
17. G. Fischer and P. Eyerer, *Polym. Comp.*, **9**, 297 (1988).
18. P.J. Hine, R.A. Duckett, N. Davidson, and A.R. Clarke, *Comp. Sci. Technol.*, **47**, 65 (1993).
19. C. Eberhardt, A. Clarke, M. Vincent, T. Giroud, and S. Flouret, *Comp. Sci. Technol.*, **61**, 1961 (2001)
20. A.R. Clarke, G. Archenhold, and N.C. Davidson, *Comp. Sci. Technol.*, **55**, 75 (1995).
21. C. Eberhardt and A. Clarke, *Comp. Sci. Technol.*, **61**, 1389 (2001).
22. L. Avérous, J.C. Quantin, A. Crespy, and D. Lafon, *Acta Stereologica*, **14**, 69 (1995)
23. L.K. Jain and R.C. Wetherhold, *Acta Metallurg. Mater.*, **40**, 1135 (1992).
24. C.L. Tucker III and E. Liang, *Comp. Sci. Technol.*, **59**, 655 (1999).
25. Y.T. Zhu, W.R. Blumenthal, and T.C. Lowe, *J. Compos. Mater.*, **31**, 1287 (1997).
26. B. Möginger and P. Eyerer, *Composites*, **22**, 394 (1991).
27. R.S. Bay and C.L. Tucker III, *Polym. Eng. Sci.*, **32**, 240 (1992).
28. B. Mlekusch, A. Lehner, and W. Geymayer, *Compos. Sci. Technol.*, **59**, 543 (1999).
29. G. Zak, C.B. Park, and B. Benhabib, *J. Compos. Mater.*, **35**, 316 (2001).
30. B. Lian, J. Ladewig, J.M. Wille, and J.J. McGrath, *Annu. Tech. Conf. SPE ANTEC.*, **II**, 2316 (1994)
31. L. Avérous, J.C. Quantin, A. Crespy, and D. Lafon, *Polym. Eng. Sci.*, **37**, 329 (1997).
32. G. Saint-Martin, F.M. Schmidt, P. Devos, and C. Levaillant, *Polym. Test.*, **22**, 947 (2003).
33. M.H. Wesselmann, *Impact of Injection Molding Conditions on the Properties of Short Fiber Reinforced High Performance Thermoplastic Parts*, Ph.D. thesis of Ecole Nationale Supérieure des Mines de Paris (2003).
34. S.W. Yurgartis, *Compos. Sci. Technol.*, **30**, 279 (1987).
35. S.W. Yurgartis, *Compos. Sci. Technol.*, **53**, 145 (1995).